Supporting information:

Exploiting Feedstock Diversity To Tune the Chemical and Tribological Properties of Lignin-Inspired Polymer Coatings

*Jillian A. Emerson,[†,‡] Nikolay T. Garabedian,[§] David L. Burris,[§] Eric M. Furst,[‡] Thomas H. Epps, III[‡,#,]**

[‡]Department of Chemical & Biomolecular Engineering, University of Delaware, 150 Academy Street, Newark, DE 19716, USA

[§]Department of Mechanical Engineering, University of Delaware, 130 Academy Street, Newark, DE 19716, USA

[#]Department of Materials Science & Engineering, University of Delaware, 127 The Green, Newark, DE 19716, USA

[†]Present Addresses: Core R&D, The Dow Chemical Company, Midland, MI 48674, USA

*Corresponding Author Email: thepps@udel.edu (T.H.E.)

Contains: 16 total pages with 7 supporting figures and 3 supporting tables.

Characterization of poly(phenyl methacrylate) [PPM] and poly(syringaldehyde methacrylate) [PSAM]

The molecular weights and dispersities of PPM and PSAM were characterized using size exclusion chromatography (SEC) in tetrahydrofuran (THF), for PPM, or chloroform ($CHCl_3$), for PSAM, see Figure S1a. The glass transition temperature (T_g) of each polymer was determined through differential scanning calorimetry (DSC) using a TA Instruments Discovery calorimeter. The T_g values presented herein for PSAM and PPM were taken from the second DSC trace on heating at 5 °C/min in N_2, see Figure S1b.

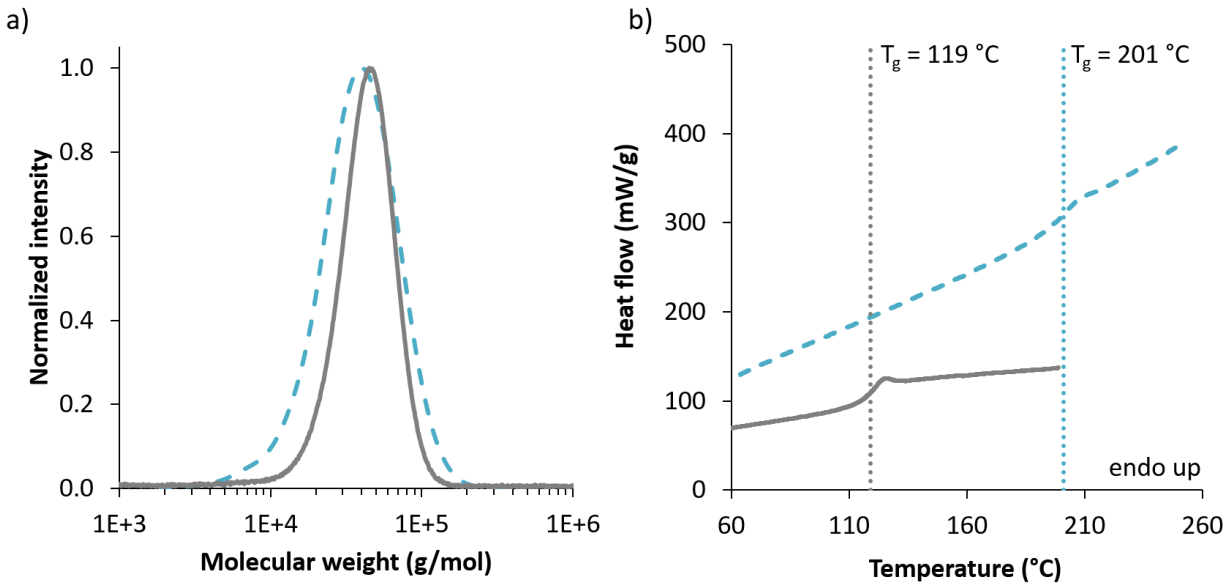

Figure S1. a) SEC trace of PPM (gray, solid) and PSAM (teal, dashed) in THF and $CHCl_3$, respectively. b) Second DSC trace on heating (endo up) of PPM (gray, solid) and PSAM (teal, dashed).

Film casting

For thinner films cast on silicon wafers (used for solvent vapor swelling and contact angle analyses), solutions of 2 wt.% polymer in anisole were prepared gravimetrically. All silicon substrates were triple-rinsed with toluene, cleaned with ultraviolet-ozone (Jelight, Model 342), and then triple-rinsed again with toluene. A flow coating apparatus was employed to cast solutions onto the cleaned silicon wafers to generate films.[1] 70 μL of solution was used to make each film. The flow coating apparatus was operated at a velocity of 17 mm/s, acceleration of 0.4 mm/s^2, gap height of 70 μm, and blade width of 15 mm to fabricate films with thicknesses >100 nm. Additional convection was applied during casting to induce directional drying, thereby producing more uniform films. The thicknesses of >100 nm were selected to remove the dependence of the measured film swelling on the initial film thickness.[2-3] For thicker films cast on silicon wafers (used for tribology experiments), solutions of 10 wt.% polymer in dichloromethane were prepared gravimetrically. These films were cast using a velocity of 12 mm/s, acceleration of 0.8 mm/s^2, blade width of 20 mm, and gap height of 70 μm, with a 50 μL solution volume to produce films >1 μm in thickness.

Solvent vapor swelling

In solvent vapor swelling, a dry polymer film was exposed to a solvent-rich atmosphere. The solvent diffused into the film and swelled the polymer chains. The amount of solvent that was incorporated into the film ($\phi_s = 1-\phi_p$, for which ϕ_p is the polymer volume fraction) depended on the solvent concentration in the chamber and the polymer-solvent Flory-Huggins interaction parameter, $\chi_{s\text{-}p}$. The solvent concentration was defined by the ratio of the pressure of solvent within

the chamber, p_i, to the saturated partial pressure at the experimental temperature, $p_{i,sat}$ (see Equation 1 in the main text).

For these swelling experiments, the total nitrogen flow rate (the sum of the solvent-rich flow rate and the nitrogen diluent flow rate) was maintained at 25 mL/min, and the solvent concentration was tuned by changing the relative flow rate between the solvent-rich stream and the nitrogen diluent stream. At each composition of solvent, the polymer film was allowed to equilibrate in the solvent atmosphere, i.e., the polymer film kept in the environment until the polymer volume fraction in the film did not change with time. After equilibration, the relative flow rates of the solvent-rich vapor stream and the nitrogen diluent stream were adjusted to reduce the solvent concentration within the chamber.

Refractive index estimation

A Veeco Dimension 3100 atomic force microscope (AFM) operated in tapping mode was used to capture the AFM micrographs. Silicon probes (tap150) with a force constant of 5 N/m and resonant frequencies between 120 kHz and 180 kHz were used to image the films. The film thicknesses were measured using a scratch test method, in which a scratch was made in the film to measure the relative height between the newly uncovered substrate and film surface.

The normal reflectance of the film was measured using a spectral reflectometer (Filmetrics, Inc. F20-UV). The reflectance curve was fit by fixing the film thickness at the value obtained from the scratch test and using the refractive index as a fitting parameter. This refractive index value was taken as the polymer film refractive index in subsequent measurements of film thickness for the solvent-swollen films. The refractive index of swollen films was approximated as the volume-weighted average of the native polymer film refractive index and the solvent refractive index.

Contact angle analysis

Contact angle measurements were obtained using a First Ten Ångstroms (FTÅ) 125 contact angle device. For each test, 2 μL of liquid was dispensed onto the film surface by a Distriman pipette. The static contact angles were recorded after the drop shape stabilized (4 s for both diiodomethane and water). The contact angles were calculated from the images using the manual points fitting algorithm in the ImageJ contact angle plugin.

Sustainable polymer friction coefficients

In addition to solubility and surface energy, the friction coefficient of the sustainable polymers can impact potential suitability for various applications. Each sample was tested with a 2 mm path length at a constant normal load of 5 mN for 100 cycles, with a velocity of 4.6 mm/s. This low velocity was selected to mitigate any effects of frictional heating.[4-5] Both glass and HDPE probes were used to measure the friction coefficient of various films. The reported friction coefficients were determined using data averaged over the steady state sliding regime, as discussed elsewhere.[6]

The time-dependent friction coefficient data are shown in Figure S2 for poly(guaiacyl methacrylate) [PGM], poly(syringyl methacrylate) [PSM], poly(vanillin methacrylate) [PVM], poly(creosyl methacrylate) [PCM], poly(4-ethyl guaiacyl methacrylate) [PEM], and PPM.

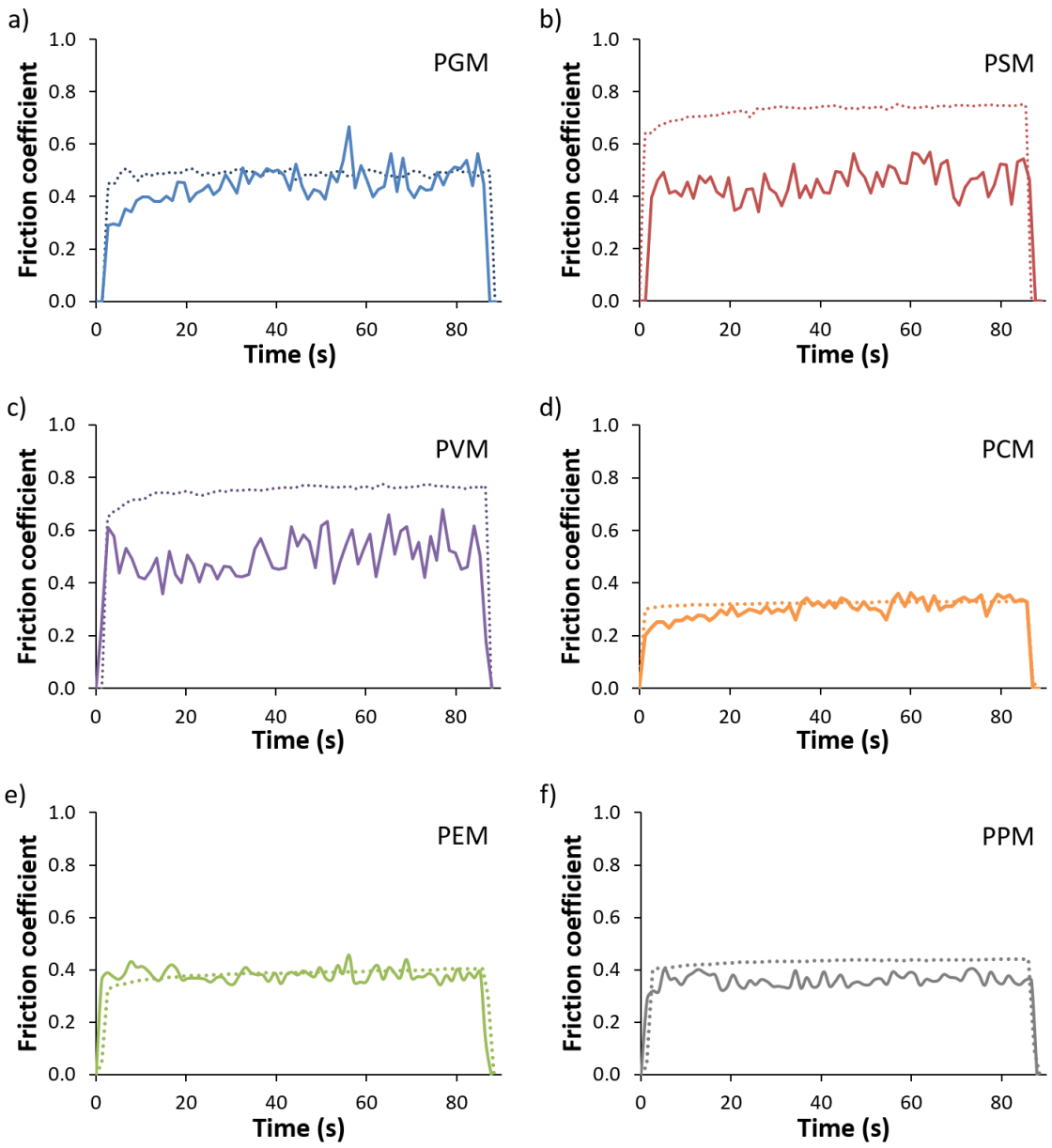

Figure S2. Friction coefficients for a) PGM, b) PSM, c) PVM, d) PCM, e) PEM, and f) PPM obtained using a glass (solid line) or HDPE (dotted line) probe. All data were obtained at a velocity of 4.6 mm/s. The friction coefficients were higher with the HDPE probe than with the glass probe for all polymers except PCM, PGM, and PEM, likely owing to the higher adhesion between the neat polymers and HDPE.

The friction coefficients were nearly independent of repeat unit structure when measured with the glass bead; however, when measured with the HDPE probe, the friction coefficients increased with oxygen content in the polymer repeat units. These data are summarized in Figure 7 of the main text and Table S1 below.

Table S1. Friction coefficient between sustainable polymer films and the glass or HDPE probe.

Polymer	**Friction coefficient (glass)**	**Friction coefficient (HDPE)**
PGM	0.46 ± 0.06	0.49 ± 0.01
PSM	0.47 ± 0.06	0.74 ± 0.00
PVM	0.53 ± 0.09	0.75 ± 0.02
PCM	0.40 ± 0.07	0.36 ± 0.07
PEM	0.42 ± 0.05	0.43 ± 0.07
PPM	0.39 ± 0.04	0.47 ± 0.05

Polymer film swelling in $CHCl_3$

The PGM films dewet under high $CHCl_3$ concentrations. This dewetting possibly was due to destabilization by short-range polar forces for the lower surface energy PGM polymer.[7-8] Although PGM was not stable enough to extract interaction parameters in $CHCl_3$, the relative swelling behavior could be used to qualitatively determine differences in compatibility. In comparison to PVM, PGM had less solvent uptake (higher polymer volume fraction). This effect suggests that PGM has less favorable interactions with $CHCl_3$ than PVM (i.e. lower solubility), as shown in Figure S3.

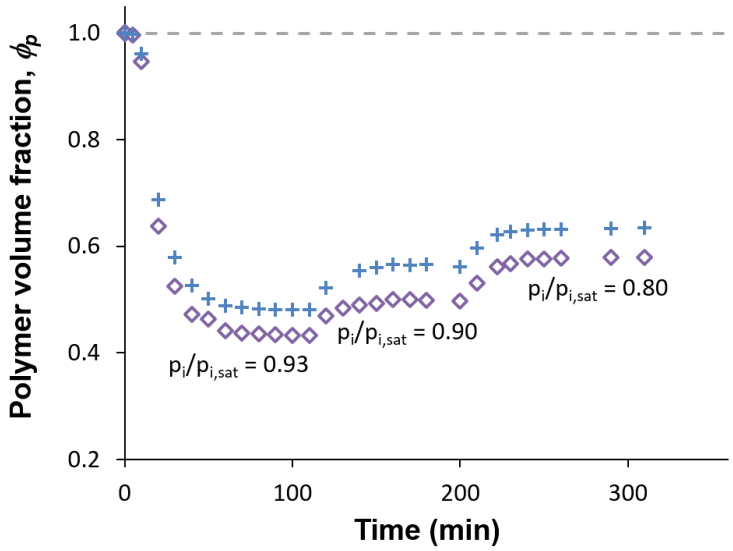

Figure S3. Comparison of temporal swelling behavior for PGM (+) and PVM (◇) as a function of $CHCl_3$ vapor concentration above the film. PGM swelled less than PVM at all $CHCl_3$ vapor compositions, which suggests that $CHCl_3$ is a better solvent for PVM than PGM.

Estimation of solvent-swollen polymer T_g

The transition between rubbery and glassy regimes was probed using the solvent vapor swelling data, shown in Figure S4, for PGM, PCM, PEM, PVM, PSM, poly(4-ethylguaiacyl methacrylate-*ran*-syringyl methacrylate) [PES], poly(creosyl methacrylate-*ran*-4-ethyl guaiacyl methacrylate-*ran*-syringyl methacrylate) [PCES], poly(vanillin methacrylate-*ran*-4-ethyl guaiacyl methacrylate-*ran*-syringyl methacrylate) [PVES], and poly(bio-oil methacrylate) [PBOM]. The intersection of the glassy and rubbery regime fits provided a critical polymer concentration, below which the polymer lacked sufficient mobility to readily equilibrate.

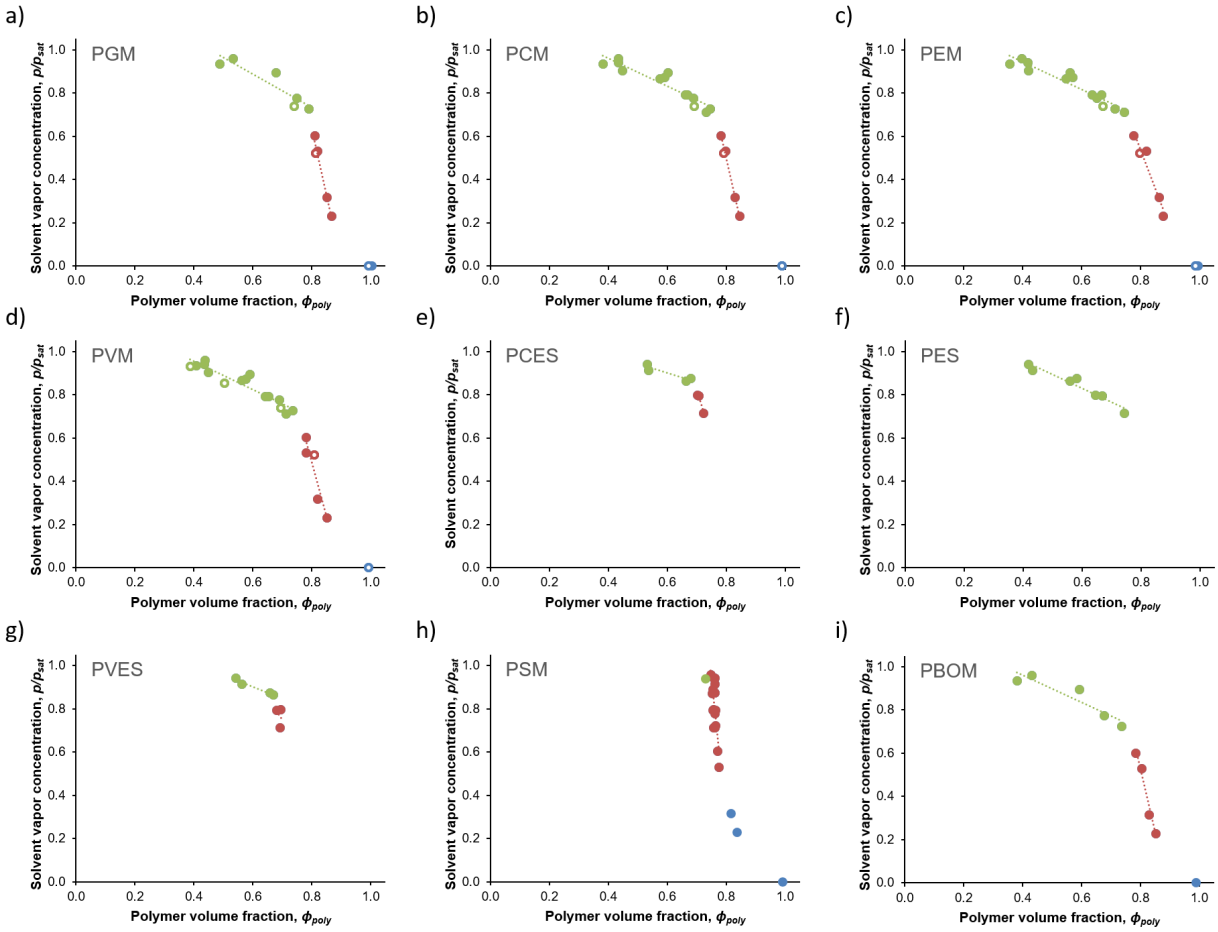

Figure S4. Effect of THF content on polymer swelling behavior for a) PGM, b) PCM, c) PEM, d) PVM, e) PCES, f) PES, g) PVES, h) PSM, and i) PBOM. Two regimes are noteworthy in the data. These regimes have been noted as 'rubbery' (●), in which the solvent uptake is less sensitive to the solvent partial pressure, and 'glassy' (●), in which the solvent uptake is more sensitive to the solvent partial pressure, as highlighted by the distinct slopes (dashed lines) in the panels. The closed symbols represent data from flow-based solvent vapor swelling experiments, whereas the open symbols represent data from THF/water bell jar swelling experiments. The blue data points represent data that were excluded from the analysis because of dissimilar swelling behavior, likely the result of startup effects. For PES, 'rubbery' behavior is noted across the THF content explored.

For PSM, 'glassy' behavior is noted across the THF content explored. The 'glassy' to 'rubbery' crossover values are listed in Table S2.

The intersection of the 'glassy' and 'rubbery' lines likely indicates the minimum polymer swelling necessary to impart the polymer chains with sufficient mobility to equilibrate with the vapor environment; this degree of swelling is referred to herein as the crossover polymer volume fraction, ϕ_c. In the literature, these types of transitions have been probed using temperature,[9] whereas, in this work, the solvent uptake is used to modify the polymer mobility.[10] Values of ϕ_c are tabulated in Table S2.

Table S2. Crossover solvent concentration, $p_{i,c}/p_{i,sat}$ and crossover polymer volume fraction, ϕ_c, from the data in Figure S4.

Polymer	$p_{i,c}/p_{i,sat}$	ϕ_c
PGM	0.75	0.78
PCM	0.73	0.76
PEM	0.72	0.75
PVM	0.72	0.75
PCES	0.88	0.66
PES	--	--
PVES	0.86	0.67
PSM	--	--
PBOM	0.67	0.77

A similar analysis was performed for select polymers in $CHCl_3$. Of particular interest is PSM when exposed to $CHCl_3$. Though limited data are available for PSM, a number of experimental conditions fell within the rubbery regime, as evidenced in Figure S5, below.

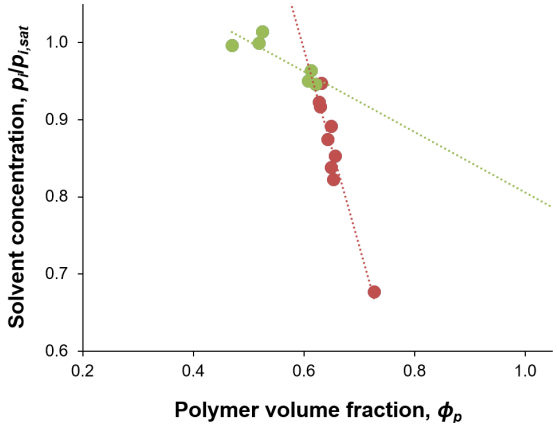

Figure S5. Effect of $CHCl_3$ content on PSM swelling behavior. In comparison to the PSM data in THF (shown in Figure S4), the PSM data in $CHCl_3$ suggest a crossover between the 'glassy' and 'rubbery' regimes.

Adhesion of polymer films

The root mean squared roughness, R_{RMS}, is given by:

$$R_{RMS} = \sqrt{\frac{1}{n}\sum d_i^2} \quad \text{eq. S1}$$

in which n is the number of pixels in the micrograph, and d_i height difference between pixel i and the mean. The roughness was characterized using AFM height images,[11] and the resulting data are presented in Figure S6.

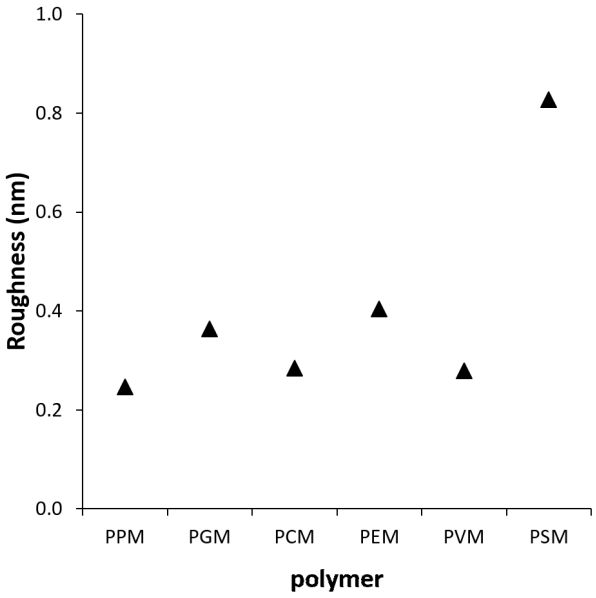

Figure S6. Root mean squared roughness of sustainable polymer films measured using AFM.

The adhesion between two surfaces was estimated from the differences in the material surface energies upon contact.[12]

$$W_{ad} = \gamma_1 + \gamma_2 - \gamma_{12} \qquad \text{eq. S2}$$

γ_i is the surface energy of material *i*, and γ_{ij} is the interfacial tension between materials *i* and *j*. The interfacial tension was determined from the geometric mean of the dispersive (γ^D) and polar (γ^P) surface energy contributions.[13-14]

$$\gamma_{12} = \gamma_1 + \gamma_2 - 2\sqrt{\gamma_1^D \gamma_2^D} - 2\sqrt{\gamma_1^P \gamma_2^P} \qquad \text{eq. S3}$$

The work of adhesion values are shown in Table S3, using the surface energies calculated from the static contact angles in Figure 6 of the main text.

Table S3. Calculated probe-film adhesion for the lignin-inspired polymers.

Polymer	$W_{glass\text{-}poly}$ mJ/m^2	$W_{HDPE\text{-}poly}$ mJ/m^2
PPM	99.7	80.6
PGM	108.9	81.1
PCM	106.4	78.6
PEM	103.4	77.4
PVM	113.9	83.4
PSM	112.7	82.9

The glass (γ^P = 80 mJ/m^2, γ^D = 32 mJ/m^2) and HDPE (γ^P = 0 mJ/m^2, γ^D = 35.3 mJ/m^2) surface energy contributions were used to calculate the work of adhesion from the sustainable polymer surface energies determined from the static contact angles with the Owens-Wendt equation.

The pull-off forces were measured for the sustainable polymers with the HDPE probe through the determination of an adhesion coefficient (i.e., the ratio of the pull-off force to the load), which could be calculated for each pull-off force and load pairing.[15] The probe was brought into contact with the surface at normal forces (loads) that varied between 0.2 mN and 12.2 mN. Probe contact and retraction rates of 1.2 μm/s, 12.0 μm/s, or 23.7 μm/s were used during adhesion testing to capture contributions from viscoelasticity.[16-18] More specifically, the adhesion coefficient was calculated by fitting a line to the normal load *vs*. pull-off force. Nearly all of the adhesion coefficients were similar within error. Minimal scatter in the data likely was a result of the very low pull-off forces (and, thus, adhesion coefficients) between the HDPE probe and the polymer films.

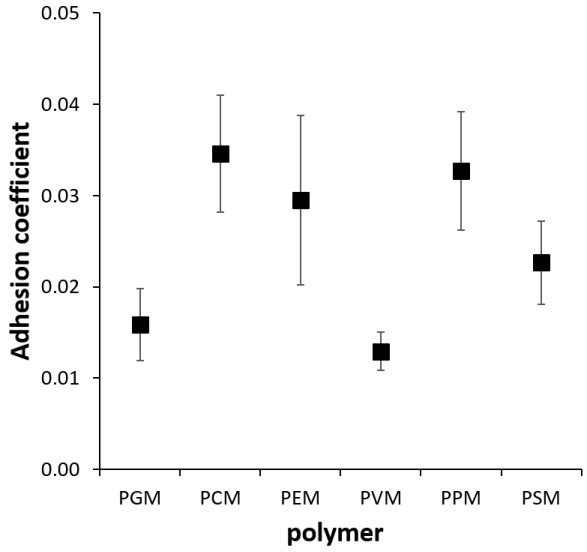

Figure S7. Adhesion coefficient for PGM, PCM, PEM, PVM, PPM, and PSM upon immediate retraction. Error bars represent the standard deviation of values obtained from multiple measurements of the same polymer film.

The adhesion coefficients for all of the polymers were low (< 0.04), and there were no apparent trends with repeat unit structure, suggesting that the changes in friction coefficients were not significantly influenced by probe-film adhesion.

REFERENCES

(1) Stafford, C. M.; Roskov, K. E.; Epps, T. H., III; Fasolka, M. J., Generating thickness gradients of thin polymer films via flow coating. *Rev. Sci. Instrum.* **2006,** *77* (2), 023908.

(2) Elbs, H.; Krausch, G., Ellipsometric determination of flory-huggins interaction parameters in solution. *Polymer* **2004,** *45* (23), 7935-7942.

(3) Manoli, K.; Goustouridis, D.; Chatzandroulis, S.; Raptis, I.; Valamontes, E. S.; Sanopoulou, M., Vapor sorption in thin supported polymer films studied by white light interferometry. *Polymer* **2006,** *47* (17), 6117-6122.

(4) McLaren, K. G.; Tabor, D., Visco-elastic properties and the friction of solids: friction of polymers: Influence of speed and temperature. *Nature* **1963,** *197* (4870), 856-858.

(5) Grosch, K. A., Visco-elastic properties and the friction of solids: relation between the friction and visco-elastic properties of rubber. *Nature* **1963,** *197* (4870), 858-859.

(6) Emerson, J. A.; Garabedian, N. T.; Moore, A. C.; Burris, D. L.; Furst, E. M.; Epps, T. H., III, Unexpected tribological synergy in polymer blend coatings: leveraging phase separation to isolate domain size effects and reduce friction. *ACS Appl. Mater. Interfaces* **2017,** *9* (39), 34480-34488.

(7) Lee, S. H.; Yoo, P. J.; Kwon, S. J.; Lee, H. H., Solvent-driven dewetting and rim instability. *J. Chem. Phys.* **2004,** *121* (9), 4346-4351.

(8) Xu, L.; Shi, T.; Dutta, P. K.; An, L., Rim instability by solvent-induced dewetting. *J. Chem. Phys.* **2007,** *127* (14), 144704.

(9) Bock, H.; Christian, S.; Knoll, W.; Vydra, J., Determination of the glass transition temperature of nonlinear optical planar polymer waveguides by attenuated total reflection spectroscopy. *Appl. Phys. Lett.* **1997,** *71* (25), 3643-3645.

(10) Vrentas, J. S.; Vrentas, C. M., Effect of glass transition on the concentration dependence of self-diffusion coefficients. *J. Appl. Polym. Sci.* **2003,** *89* (6), 1682-1684.

(11) Menezes, P. L.; Kailas, S. V., Role of surface texture and roughness parameters on friction and transfer film formation when UHMWPE sliding against steel. *Biosurf. Biotribol.* **2016,** *2* (1), 1-10.

(12) Israelachvili, J. N., *Intermolecular and Surface Forces*. 3rd ed.; Academic Press: San Diego, 2011, p 415-467.

(13) Fowkes, F. M., Attractive forces at interfaces. *Ind. Eng. Chem.* **1964,** *56* (12), 40-52.

(14) Wu, S., Calculation of interfacial tension in polymer systems. *J. Polym. Sci., Part C: Polym. Symp.* **1971,** *34* (1), 19-30.

(15) Bhushan, B., *Nanotribology and Nanomechanics: An Introduction*. Springer Berlin Heidelberg: 2008.

(16) Tiwari, A.; Dorogin, L.; Bennett, A. I.; Schulze, K. D.; Sawyer, W. G.; Tahir, M.; Heinrich, G.; Persson, B. N. J., The effect of surface roughness and viscoelasticity on rubber adhesion. *Soft Matter* **2017,** *13* (19), 3602-3621.

(17) Hammerschmidt, J. A.; Gladfelter, W. L.; Haugstad, G., Probing polymer viscoelastic relaxations with temperature-controlled friction force microscopy. *Macromolecules* **1999,** *32* (10), 3360-3367.

(18) Grosch, K. A., The relation between the friction and visco-elastic properties of rubber. *Proc. R. Soc. London, Ser. A* **1963,** *274* (1356), 21-39.